JPE 16-3-14

http://dx.doi.org/10.6113/JPE.2016.16.3.960
ISSN(Print): 1598-2092 / ISSN(Online): 2093-4718

Grid-friendly Control Strategy with Dual Primary-Side Series-Connected Winding Transformers

Jing Shang†, Xiaohong Nian*, Tao Chen**, and Zhenyu Ma**

†,*School of Information Science and Engineering, Central South University, Changsha, China
**CRRC Zhuzhou Institute Co., Ltd., Zhuzhou, China

Abstract

High-power three-level voltage-source converters are widely utilized in high-performance AC drive systems. In several ultra-power instances, the harmonics on the grid side should be reduced through multiple rectifications. A combined harmonic elimination method that includes a dual primary-side series-connected winding transformer and selective harmonic elimination pulse-width modulation is proposed to eliminate low-order current harmonics on the primary and secondary sides of transformers. Through an analysis of the harmonic influence caused by dead time and DC magnetic bias, a synthetic compensation control strategy is presented to minimize the grid-side harmonics in the dual primary side series-connected winding transformer application. Both simulation and experimental results demonstrate that the proposed control strategy can significantly reduce the converter input current harmonics and eliminates the DC magnetic bias in the transformer.

Key words: Dead time, Harmonic, Magnetic-bias, Series-connected, SHEPWM, Transformer

I. INTRODUCTION

Active rectifiers that can feed back the breaking energy to the grid are commonly employed in high-power drive systems, such as metallurgical rolling mills and mines. In medium-voltage applications, active rectifiers often adopt a three-level neutral-point-clamped topology with the merits of high voltage and low harmonics. However, in this case, the converter must be controlled with low switching frequency considering the switching losses. The reduction in current harmonics with a low switching frequency is an important issue in the design of high-power converter systems.

The modulation methods and control strategies [1]-[8] of three-level converters have long been a research issue. Many scholars have exerted fruitful efforts to reduce grid-side harmonics significantly. Most of them focused on modulation strategy and system design and implemented comprehensive optimization. The specific harmonics-eliminating modulation strategy [selective harmonic elimination pulse-width modulation (SHEPWM)] is a preferable modulation method at low switching frequency with low grid current total harmonic distortion (THD). A type of three-level SHEPWM strategy was presented in [9]. The strategy can realize balance in neutral voltage. A certain minimum harmonic modulation strategy that can achieve the most optimal harmonic modulation ratio in the entire scope was also proposed in [10]. These studies focused on the theory analysis of a single aspect of the SHEPWM strategy under ideal conditions.

In practical applications, for the design of a grid-side system, the structure of the transformer directly affects the grid-side harmonics. For example, the split-type pulse transformer, which is widely utilized in urban rail transit power systems, can effectively eliminate the primary-side current harmonics of the transformer. [11], [12] proposed a three-level harmonic optimal modulation strategy based on a 12-pulse rectifier transformer integrated with a dual main circuit structure. This strategy can realize low harmonics in the transformer primary side with low switching frequency. A multiple-tandem transformer winding structure was described in [13], [14]. This structure is mainly utilized for high-voltage DC power systems and static

Manuscript received Sep. 7, 2015; accepted Jan. 9, 2016
Recommended for publication by Associate Editor Honnyong Cha.
†Corresponding Author: shangjing@teg.cn
Tel: +86-0733-28494371, Fax: +86-0733-28494371, Central South University
*School of Information Science and Eng., Central South Univ., China
**CRRC Zhuzhou Institute Co., Ltd., China

synchronous compensators. However, the working principle, advantages, and output current harmonic characteristics of the system on the grid side were not analyzed comprehensively.

The dead time of a high-power device influences the control precision and voltage harmonic distribution in the converter output valve-side fundamental wave. In addition to several non-ideal factors, such as the influence of grid voltage harmonics and the difference in device switch characteristic and control system error, the magnetic bias in the transformer windings caused by the DC component of the pulse-width modulation (PWM) converter output voltage [15]-[18] also leads to grid-side current distortion and affects the grid-side current harmonics. [19]-[21] discussed the influence of dead time and compensation strategies; space vector PWM was used in detail. [22]-[24] proposed several control strategies to inhibit magnetic bias, but they focused on carrier modulation and square wave modulation strategies. In low-switching-frequency applications, the dead time effect of SHEPWM for three-level converters and the corresponding magnetic bias compensation methodology have not been reported to date.

A combined harmonic elimination method that includes a dual primary-side series-connected winding transformer and SHEPWM is introduced in this study to eliminate the low-order harmonics of the primary-side and secondary-side currents of the transformer. The effects of dead time and magnetic bias are analyzed in principle. A synthetic compensation control strategy (SHEPWM-SC) is then proposed to minimize the grid-side harmonics in the dual primary-side series-connected winding transformer application. Finally, experiments are conducted on the dual primary series-connected winding transformers based on three-level integrated gate communicated thyristor (IGCT) converters. Both simulation and experimental results show that the proposed control strategy can eliminate $12k \pm 1 (k = \frac{T-1}{2})$ order harmonics and below and can further reduce grid harmonics by dead time and magnetic bias compensation.

II. COMBINED HARMONIC ELIMINATION

As an important system component, the structure and design parameters of the transformer directly determine the converter performance level in the system design. The multiple-primary-side series-connected winding transformer, as a special transformer structure, is mainly utilized in high-power systems [25–27]. Compared with the multiple-split winding transformer, a lower short-circuit impedance of the multiple-primary-side series-connected winding transformer can be designed but with the same current THD. Thus, the transformer size can be reduced. The secondary-side current of the split winding transformer contains abundant harmonics when connected to a high-power converter. However, the primary current harmonic can be at a low level by carrier-phase shifting or transformer wind shifting. The structure of the primary-side series-connected winding transformer reveals that

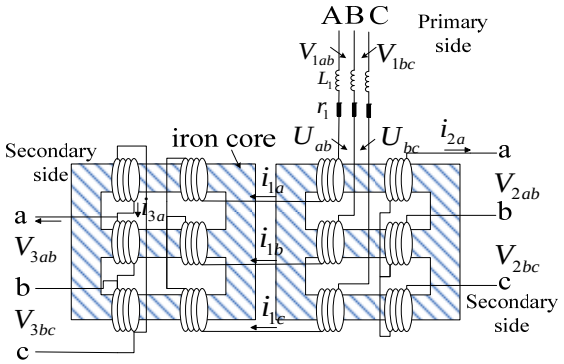

Fig. 1. Schematic of the transformer.

the current harmonic level is similar in both windings; only the amplitude differs. After applying a certain control strategy, the current harmonic on both sides can be at a low level. The waveform factor is optimized, and capacity is fully maximized.

A schematic of a dual series-connected winding transformer is shown in Fig. 1. The primary and secondary windings of dual transformers are connected in star (Y) and delta (Δ) forms. The dual secondary windings are connected separately to the as sides of PWM converters. Transformer leakage inductors are utilized as the input inductors. The voltages/currents in the dual secondary windings have a 30° phase shift.

In Fig. 1, a, b, and c are the three input phases of the converter. V_{1ab}, V_{1bc} are the line voltages on the grid side. V_{2ab}, V_{2bc} are the line voltages of the secondary Y-connected winding. V_{3ab}, V_{3bc} are the line voltages of the secondary Δ-connected winding. U_{ab}, U_{bc} are the primary-side line voltages inducted from the secondary winding. i_{1a} , i_{1b} , i_{1c} are the Phase A, B, and C primary side currents, i_{2a} is the Phase A current of the secondary Y-connected winding, i_{3a} is the Phase A current of the secondary Δ-connected winding, and L_1 and r_1 are the equivalent impendence of the transformer winding.

We let the turn ratios of the primary and secondary windings be k_1 and k_2 to guarantee the consistency of the two secondary voltages. The turn ratios of the two windings satisfy the relationship

$$\frac{k_1}{\sqrt{3}} = k_2 = f. \tag{1}$$

Given the special structure of the transformer, a strong coupling relationship exists within the windings. The output voltages of PWM rectifiers connected to the dual secondary windings have the same magnitude but a 30° phase shift to maintain current and voltage sharing within the windings. By analyzing the output line voltages of the dual converters, we can rewrite the inverter output voltage as follows:

$$V_{2ab} = \sum_{n=1,5,7,11,13,\ldots\ldots}^{\infty} \hat{V}_n \sin(n\omega t + \varphi_n) \text{ and}$$

$$V_{3ab} = \sum_{n=1,5,7,11,13,\ldots\ldots}^{\infty} \hat{V}_n \sin[n\left(\omega t + \frac{\pi}{6}\right) + \varphi_n],$$

where $\hat{V}_n$ is the amplitude of each harmonic in line voltage and φ_n is the initial phase of each harmonic in Y-connected winding line voltage.

Therefore,

$$U_{ab} = 2\sqrt{3}f[\hat{V}_1 sin(\omega t + \varphi_1) + \sum_{n=12k\pm1}^{\infty} \hat{V}_n sin(n\omega t + \varphi_n)], \quad (2)$$

where k=1,2,3……, U_{ab} is the primary-side Line AB voltage inducted from the secondary winding.

As indicated by Equ. 2, the primary-side line voltage U_{ab} inducted from the secondary PWM voltage of the transformer only contains $12k\pm1$ (k=1,2,3……)-order harmonic components. When using SHEPWM,

$$\begin{cases} \sum_{k=1}^{N}(-1)^{k+1} cos\,\alpha_k = M \\ \sum_{k=1}^{N}(-1)^{k+1} cos\,n\alpha_k = 0 \quad n = 11,13,23,25\ldots\ldots \end{cases}, \quad (3)$$

where M is the modulation ratio and α_k is the switching angle in a quarter of a switching cycle.

If the switching frequency is T (T is odd) times of the power frequency (50 Hz), the $12k\pm1$ (k=1,2,3……$\frac{T-1}{2}$) harmonics can be eliminated in Line AB voltage. Accordingly,

$$U_{ab} = 2\sqrt{3}f[\frac{2\sqrt{3}MU_{DC}}{\pi} sin(\omega t + \varphi_1) + \sum_{n=12k\pm1}^{\infty} \hat{V}_n sin(n\omega t + \varphi_n)], \quad (4)$$

where $k = \frac{T+1}{2}, \frac{T+1}{2}+1, \frac{T+1}{2}+2\ldots\ldots$ and U_{dc} is the DC link voltage.

Line BC voltage U_{bc} inducted from the secondary winding is similar to that in Equ. 4.

For the primary current, the equation can be written as

$$\begin{cases} \frac{di_{1a}}{dt} = -\frac{r_1}{L_1} i_{1a} + \frac{2}{3L_1}(V_{1ab} - U_{ab}) + \frac{1}{3L_1}(V_{1bc} - U_{bc}) \\ \frac{di_{1b}}{dt} = -\frac{r_1}{L_1} i_{1b} - \frac{1}{3L_1}(V_{1ab} - U_{ab}) + \frac{1}{3L_1}(V_{1bc} - U_{bc}) \end{cases},$$

where i_{1a} is the Phase A primary-side current, i_{1b} is the Phase B primary-side current, V_{1ab} is the Line AB voltage on the grid side, and V_{1bc} is the Line BC voltage on the grid side.

If the grid voltage is ideal, the primary-side phase current i_1 from the above equations only contains $12k \pm 1 (k = \frac{T+1}{2}, \frac{T+1}{2}+1\ldots\ldots)$ harmonics, and the secondary phase current can be written as

$$\begin{cases} i_{2a} = k_1 i_{1a} \\ i_{3a} = k_2 i_{1a} \end{cases}.$$

Therefore, the secondary winding phase currents i_{2a} and i_{3a} of the transformer contain $12k \pm 1 (k = \frac{T+1}{2}, \frac{T+1}{2}+1\ldots\ldots)$-order harmonics, from which the current harmonics on each side of the transformer can be eliminated. The waveform coefficient of the converter input current is improved, which is friendly to the grid.

III. Dead Time and Magnetic Bias

A. Influence of Dead Time

Dead time τ must be inserted in the complementary pulse trigger signal to guarantee that the same phase switch can reliably turn off to prevent the shoot-through phenomenon. Owing to the characteristic of the turn-on and turn-off snubber circuit, high-power semiconductor devices (such as IGCT) need longer dead time. Therefore, the effect of dead time remains severe although switching frequency is low.

High-power electric drive converters always operate in unit power factor. When the motor operates in motor mode, current and voltage have the same phase on the grid side. When the motor operates in generator mode, current and voltage have an opposite phase. The dead time effects on the phase voltage of the converter when using SHEPWM are shown in Fig. 2. In Fig. 2(a), the system works as a rectifier, and dead time leads to a wide pulse width of the ideal phase voltage level. In Fig. 2(b), the system works as an inverter, and dead time leads to a narrow pulse width of the ideal phase voltage level.

The actual output voltage of the converter is as follows:

$$U'_{po} = \begin{cases} U_{po} + U_{gain} & i \text{ and } U_{po} \text{ in the same phase} \\ U_{po} + U_{lose} & i \text{ and } U_{po} \text{ in the reverse phase} \end{cases},$$

where U'_{po} is the actual phase voltage, U_{po} is the ideal phase voltage, U_{gain} is the voltage gain caused by dead time, U_{lose} is the voltage loss caused by dead time, and i is the input current on the grid side.

Under the condition of the rectifier mode, with the effect of dead time as an example, after Fourier transform for the periodic function, we obtain

$$U_{gain}(t) = \frac{a_0}{2} + \sum_{n=1}^{\infty}(a_n cos\,n\omega t + b_n sin\,n\omega t),$$

Where

$$\begin{cases} a_0 = 0 \\ a_n = -\frac{U_{DC}}{n\pi}[sin\,n\tau \sum_{k=1}^{N}(-1)^{k+1} cos\,n\alpha_k - (1 - cos\,n\tau)\sum_{k=1}^{N} sin\,n\alpha_k] \\ b_n = -\frac{U_{DC}}{n\pi}[(1 - cos\,n\tau)\sum_{k=1}^{N}(-1)^{k+1} cos\,n\alpha_k - sin\,n\tau \sum_{k=1}^{N} sin\,n\alpha_k] \end{cases}. \quad (5)$$

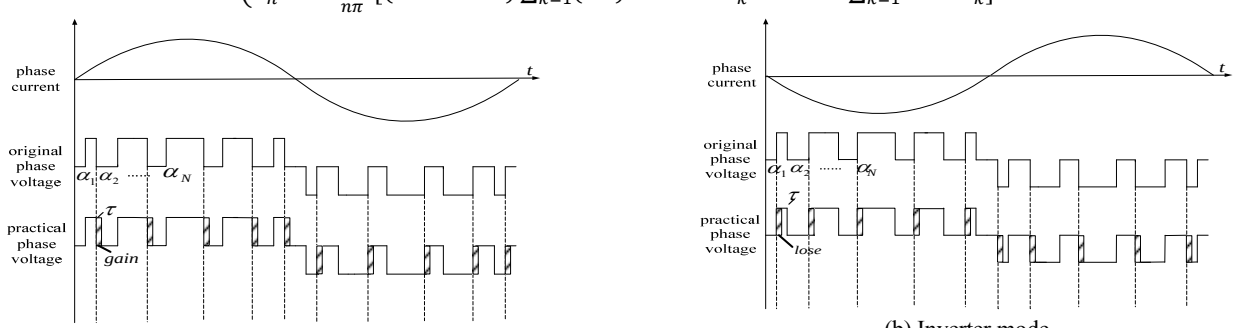

(a) Rectifier mode. (b) Inverter mode.

Fig. 2. Effect of dead time on phase voltage.

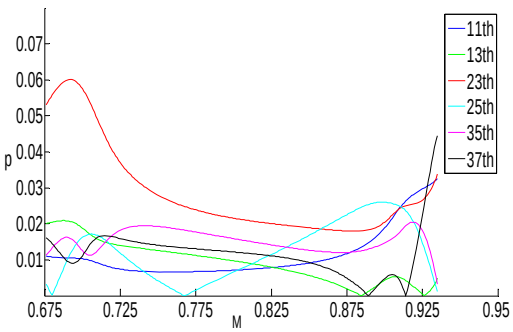

(a) p/M change curve in 60 μs dead time.

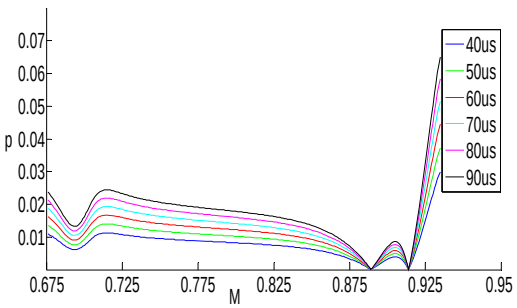

(b) 37th harmonic/M change curve at different dead times.

Fig. 3. Dead time effects.

Given that $U_{gain}(t)$ is an odd function, no even-order harmonic components exist in it. For SHEPWM, by substituting Equ. 3 into Equ. 5, we can calculate the harmonic amplitudes as

$$\sqrt{a_n^2 + b_n^2} = \frac{\sqrt{2}U_{DC}}{n\pi}\sqrt{1 - cos\, n\tau}\,|\sum_{k=1}^{N} sin\, n\alpha_k\,|. \qquad (6)$$

The harmonic phase is provided by

$$arctan\frac{a_n}{b_n} = arctan\frac{1-cos\, n\tau}{sin\, n\tau}.$$

If the switch frequency is 350 Hz, it works in a normal modulation scope (0.675<*M*<0.934). We net *n*=11, 13, 23, 25, 35, 37 in Equ. 5. The converter works in the rectifier state, and the dead time effects on each harmonic are shown in Fig. 3.

In Fig. 3(a), *p* is the proportion of harmonic amplitude and half voltage and *M* is the modulation ratio. Given that the dead time is fixed, the effects of dead time on each harmonic amplitude of phase voltage are different. In the normal modulation ratio, the *23rd* harmonic that should be eliminated is up to 6% of a half bridge voltage amplitude, the *37th* harmonic reaches 4%, and the others increase at different degrees.

By Equ. 6, along with the increase in dead time, the harmonic amplitudes in every phase voltage increase. With the *37th* harmonic as an example, as shown in Fig. 3(b), harmonic amplitude increases with dead time. When the dead time reaches 90 μs, the *37th* harmonic's amplitude can reach 6.5% of the half bridge voltage, which results in increased current harmonic on the grid side

B. Influence of Magnetic Bias

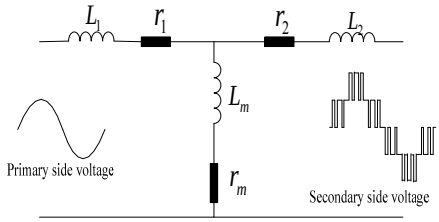

Fig. 4. Single-phase model of a transformer.

For high-power three-level converters, the input inductor on the grid side is generally equivalent to the leakage inductor of transformers. A single-phase model of a transformer is shown in Fig. 4. The transformer secondary side is usually directly connected to the converter valve side. Thus, PWM voltage directly imposes on the transformer secondary side. Owing to the sampling bias of the control system, delay characteristics, power grid voltage harmonics, and semiconductor voltage drop, the PWM voltage on the valve side contains a DC component, which causes the transformer core to become saturated over a long period and leads to current distortion on the transformer secondary side.

L_m and r_m are the magnetizing impedance of the transformer.

Magnetic induction intensity *B(t)* can be written as

$$B(t) = \int \frac{U_1}{N_1 S} dt,$$

where U_1 is the voltage on the valve side of the converter, N_1 is the number of turns on the secondary side of the transformer, and *S* is the effective cross-sectional area of the transformer core.

We let

$$U_1 = U_{AC} + U_{DC},$$

where U_{AC} represents the AC component of the converter voltage on the valve side and U_{DC} is the DC component.

Hence,

$$B(t) = \int \frac{U_{AC}}{N_1 S} dt + \int \frac{U_{DC}}{N_1 S} dt. \qquad (7)$$

From Equ. 7, when U_{DC}=0, the V–S area is equal to the forward and reverse pulse as well as the maximum operating magnetic induction intensity, as shown in Fig. 5. The magnetic core operating point moves along the hysteresis loop symmetrically and without biasing. In several cases, if U_{DC}>0, the V–S area of the positive pulse is larger than that of the reverse pulse and the maximum magnetic induction intensity. The hysteresis loop in the entire pulse cycle transfers to the first quadrant and thus results in biasing.

In the subsequent cycle, when the time difference ceases to increase, the bias does not increase either. However, the bias cannot be eliminated automatically. When the magnetic bias increases sequentially, the magnetic core saturates, and the nonlinearity of the magnetic curve increases. The magnetizing current increases rapidly and leads to transformer saturation eventually, which then causes a sharp increase in current through the transformer. This part of sharp-increased current is superimposed on the secondary side of the transformer current

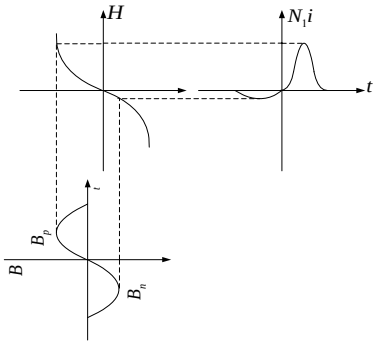

Fig. 5. Transformer DC bias magnetic saturation.

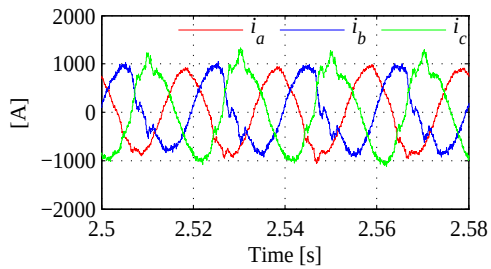

(a) Converter input current.

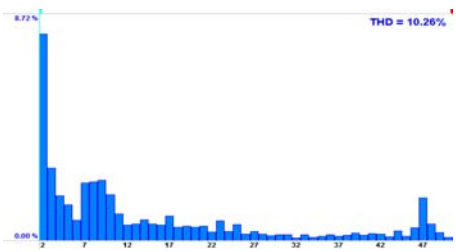

(b) Spectrum diagram of phase current.

Fig. 6. Transformer magnetic bias saturation.

and causes current distortion and deterioration of the grid-side harmonic. The analysis of the DC component is similar, and no additional details are provided.

In a three-phase transformer, any DC component existing in line voltage leads to magnetic bias corresponding to the two phases of the transformer and causes serious current distortion.

The waveform of the grid-side input current when magnetic bias saturation occurs is shown in Fig. 6(a). Converter three-phase current distortion occurs periodically at the wave crest and trough, where a sharp current slew rate di/dt results in overvoltage and damages the devices severely in extreme situations.

Fig. 6(a) presents the converter three-phase input currents. Fig. 6(b) shows the fast Fourier transform analysis of Phase A current. According to Fig. 6(b), transformer magnetic bias saturation brings considerable low-order current harmonics to the grid, especially even-order harmonics. Asymmetric even-order harmonics are introduced to the modulation wave by feedback control, which increases the DC component in the modulation wave. This increase leads to further asymmetry of the output pulse in the control system. Therefore, once the transformer magnetic bias saturates, positive feedback may be caused by the asymmetric even-order harmonics in the output current, which enhance the transformer magnetic bias in turn.

IV. Proposed Control Strategy

Given the special structure of the transformer, a strong coupling relationship exists within windings. Voltage and current sharing must be maintained within windings. Particularly in high-voltage cases, dead time and magnetic bias exert significant effects on the system. Therefore, traditional multiple current loop and inverter control are unsuitable for this system. In this section, a synthetic compensation control strategy called SHEPWM-SC that includes combined harmonic elimination, dead time, and magnetic bias compensation is proposed to minimize the harmonics with dual series-connected winding transformers. The structure of the proposed control strategy is shown in Fig. 7.

In an ideal transformer model, the secondary-side phase current is proportional to the primary-side phase current, and any change in one current will affect the other current. Unlike the traditional multiple-split transformer winding that is decoupled, the secondary windings of the dual primary-side series-connected winding transformer have a strong coupling relationship. The dual winding inducted to the primary voltage and current should present strict equilibrium. Otherwise, the primary winding voltage will become unbalanced. Consequently, traditional utility voltage outer loop and independent current inner loop control are no longer feasible. In an ideal condition, the secondary-side currents i_2 and i_3 have the same controlled quantity. Taking the dual current into three-phase average dq transformation and making feedback control with instantaneous average current will transform the inner current closed-loop output quantity into a three-phase modulation wave. After phase shift, a dual grid-side converter module control pulse is generated. This pulse can ensure strict equalization between dual windings. The sampling signal of voltage and current on the grid side must pass through a filter to reduce the adverse influence of the grid-side harmonics in voltage and current feedback on control performance. Through a control diagram, the DC voltage is controlled by active current I_d, and the power factor is controlled by reactive current I_q. When the reactive current is 0, the system works in unit power factor.

The primary-side and secondary-side currents only contain $12k \pm 1 (k = \frac{T+1}{2}, \frac{T+1}{2} + 1 \ldots\ldots)$-order harmonics by using combined harmonic elimination. As for dead time and magnetic bias compensation, no details are provided in this paper in consideration of limitations in space.

V. Simulation Results

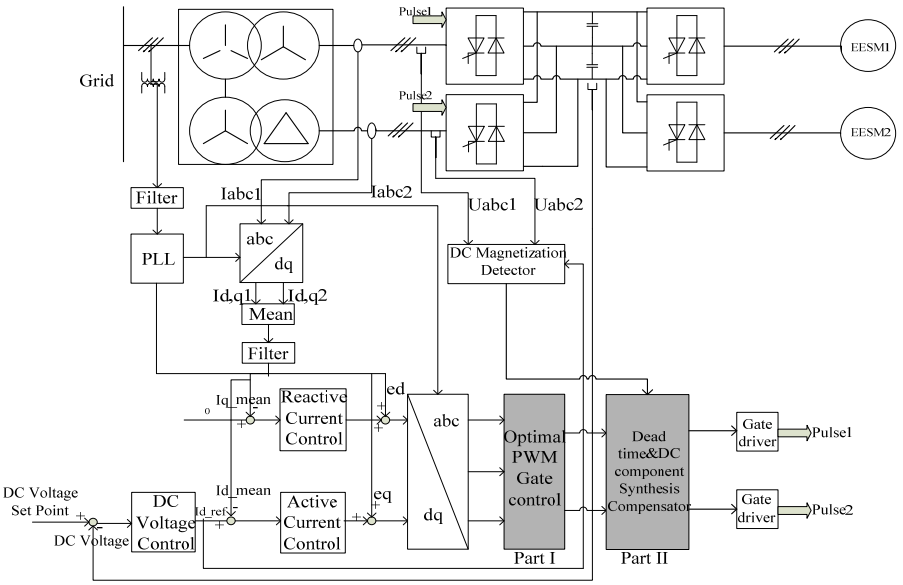

Fig. 7. Proposed control structure.

A simulation model is built in Matlab to validate the proposed control strategy. The transformer parameters are as follows: the capacity is 13.6 MVA, dual primary-side series-connected winding is adopted, the valve-side windings are Y-connected and Δ-connected with their short-circuit impedances (12%), and the output voltage of the valve-side windings is 3.16 kV. The DC-link voltage is 4840 V. The switching frequency is 350 Hz, and the dead time is 60 μs (depending on the characteristics of IGCT and the snubber circuit).

The three-phase output current waveforms of the Y-connected winding with SPWM, SHEPWM-DC (SHEPWM with magnetic bias compensation), and SHEPWM-SC are shown in Fig. 8. Their $12n\pm1$ (n=1,2,3) harmonic values are listed in Table I. The SPWM technique presents much larger *11th* and *13th* output current harmonic values than SHEPWM-DC and SHEPWM-SC. The amplitude of each harmonic component of SHEPWM-SC is smaller than the others.

Control system sampling errors, data transmission delay, device characteristics, and other factors result in a DC offset in the converter output voltage. The influence of the DC offset on the transformer magnetic bias hardware in the loop simulations with dSPACE is verified.

Fig. 9 shows a diagram of the hardware-in-loop setup of the three-level medium-voltage transmission system. The setup is built in crate, and a digital signal processor and a field-programmable gate array are used to achieve the control algorithm. The transformer, electric motor, converter, power grid, and complete set of transmission system mathematical models are built with dSPACE.

The magnetic flux-exciting current of the transformer

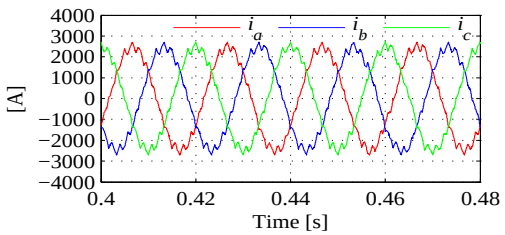

(a) PWM.

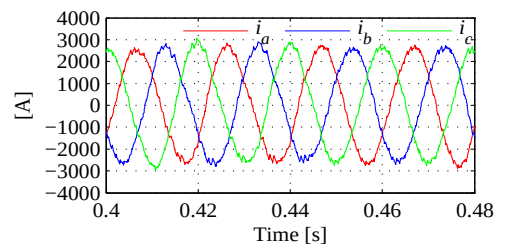

(b) SHEPWM-DC.

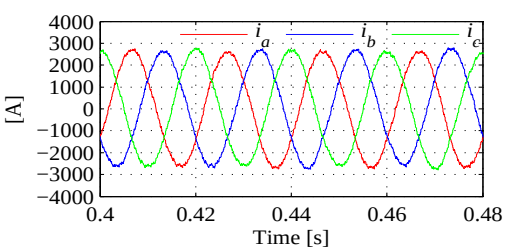

(c) SHEPWM-SC.

Fig. 8. Output current waveforms of the Y winding.

characteristic curve is shown in Fig. 10. When magnetic flux is located in the rated area, the exciting current of the transformer is far below the rated current. Once magnetic flux is saturated, the exciting current of the transformer would increase sharply, which generates output current distortion.

Fig. 11(a) shows the Y-connected winding exciting current waveforms using SHEPWM without compensation. The

TABLE I
OUTPUT CURRENT HARMONIC VALUE OF Y WINDING (FUNDAMENTAL WAVEFORM VALUE 2600A) WITH SPWM, SHEPWM-DC, AND SHEPWM-SC

	SPWM	SHEPWM-DC	SHEPWM-SC
Order	**Harmonic amplitude (A)**	**Harmonic amplitude (A)**	**Harmonic amplitude (A)**
11	102.73	6.24	3.23
13	83.56	7.98	4.48
23	22.15	15.33	1.99
25	2.70	6.15	0.43
35	8.15	12.67	1.53
37	5.08	3.94	2.31

Fig. 9. Hardware-in-loop setup of the three-level medium-voltage transmission system.

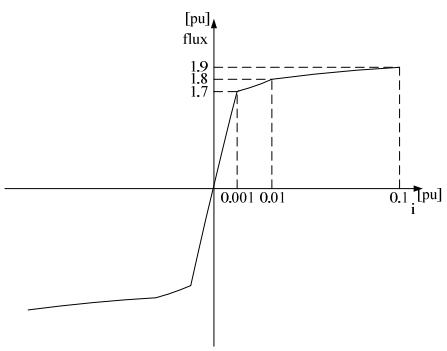

Fig. 10. Magnetic flux-exciting current of the transformer characteristic curve.

winding exciting current mutates because of flux saturation, and its peak value reaches 300 A. The output current is distorted because of the exciting current effect, as shown in Fig. 11(b).

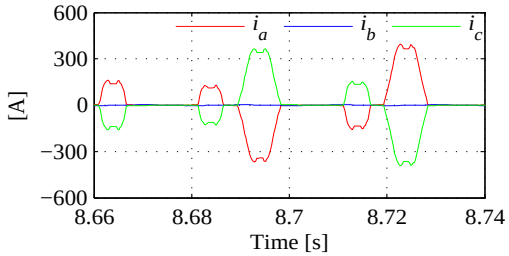

(a) Y-connected winding exciting current waveforms.

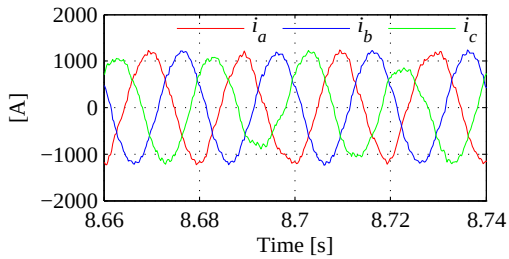

(b) Y-connected winding output current waveforms.

Fig. 11. Y-connected winding exciting current and output current with SHEPWM without compensation.

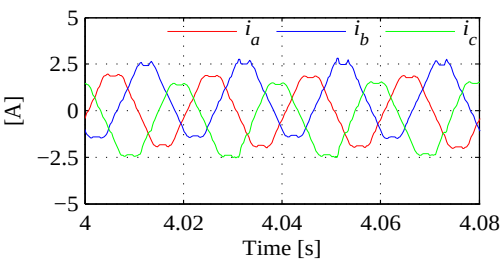

(a) Y-connected winding output current waveform

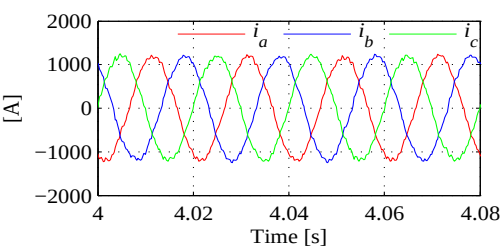

(b) Y-connected winding output current waveform.

Fig. 12. Y-connected winding exciting current and output current with SHEPWM-SC.

With the SHEPWM-SC technique, the Y-connected winding exciting current peak value is 2.5 A, which is 0.1% of the rated value without mutation presented in Fig. 12(a). Its output current has no distortion in Fig. 12(b). The transformer operates in a regular scope.

Comparative analysis of Figs. 11 and 12 shows that the DC component of PWM voltage is restrained when the SHEPWM-SC scheme is employed. The transformer magnetic flux is not saturated, and the output current exhibits no distortion.

(a) Converters. (b) Transformer.

Fig. 13. Application environment.

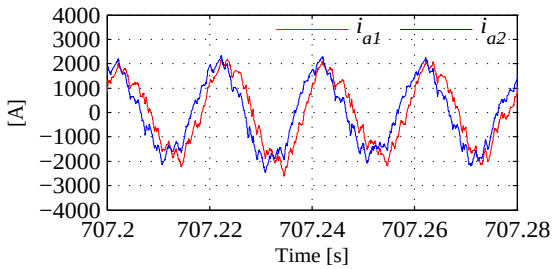

Fig. 14. Phase A output current of secondary windings with SPWM.

VI. Experimental Results

Experiments are conducted in a practical engineering application to validate the control strategy (Fig. 13). The two three-level IGCT converters have a common DC bus drive and two synchronous motors. The motor-rated power is 5 MW, and the overload is 200%.

The main technical parameters of the application are as follows:

1) transformer output voltage: 3.16 kV
2) switching frequency: 350 Hz
3) DC-link voltage: 4840 V
4) dead time: 60 μs
5) short-circuit impedance of the transformer: 7.5%

where i_{a1} is the Y-connected winding Phase A output current and i_{a2} is the Δ-connected winding Phase A output current. Fig. 14 shows the output current of transformer secondary windings with SPWM in a heavy load case. The Phase A current of the Δ-connected winding is 30° greater than the Phase A current of the Y-connected winding. The current peak value is 2000 A. According to Y-connected winding current i_{a1}, a 400 A ripple in the current peak will affect the capacity utilization of the converter in heavy-load conditions.

Figs. 15(a) and 15(b) show that the transformer output current is severely mutated under no-load and heavy-load conditions when SHEPWM without compensation is used. The ripple peak value reaches 350 A. In view of three-phase equilibrium, the other two phases are affected as well. i_b and i_c in Fig. 15(a) mutate simultaneously, which indicates that the DC component of output line voltage U_{bc} generates magnetic bias in Phases B and C. Therefore, the exciting current increases sharply. In Fig. 15(b), Phase C current mutation emerges at the fundamental wave peak point.

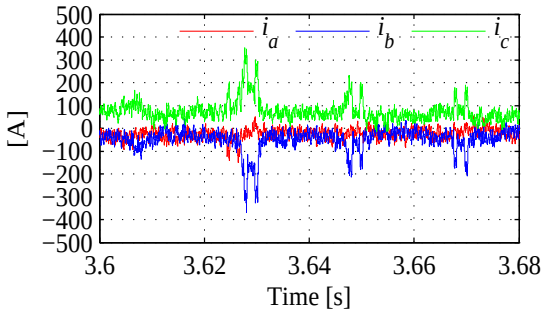

(a) SHEPWM without compensation in no load.

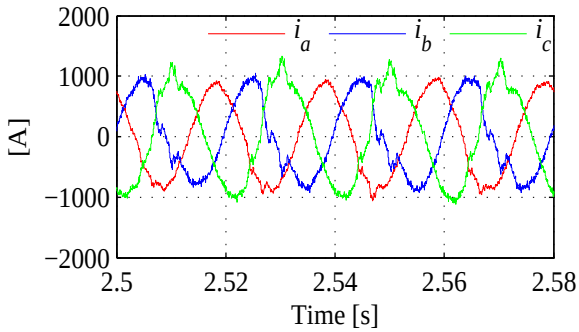

(b) SHEPWM without compensation in heavy load.

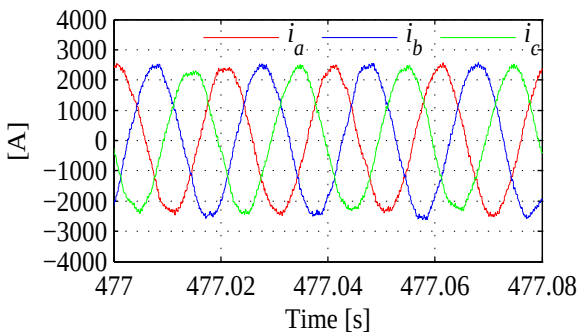

(c) SHEPWM-DC in heavy load.

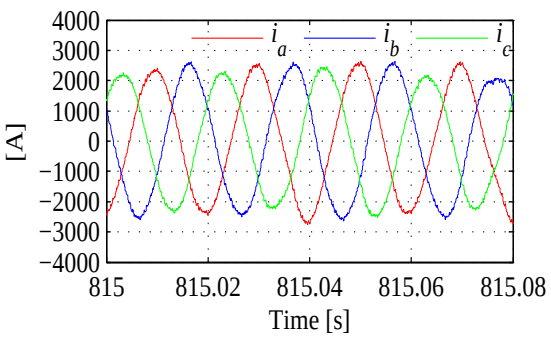

(d) SHEPWM-SC in heavy load.

Fig. 15. Output current.

The triggered convert over-current protection is probably an adverse factor for conversion reliability and safety operation in heavy-load conditions.

The output current of Y-connected winding with the SHEPWM-DC control scheme is shown in Fig. 15(c). The peak value of the input current of the converter reaches 2500

TABLE II
CURRENT HARMONIC AMPLITUDES WITH SPWM, SHEPWM-DC, AND SHEPWM-SC

Harmonics	SPWM	SHEPWM-DC	SHEPWM-SC
11	126.55	12.53	6.812
13	90.782	3.239	2.596
23	25.945	11.67	5.27
25	4.707	3.876	2.563
35	5.933	10.16	4.517
37	7.517	10.02	4.196

A. No mutation occurs in the heavy-load case. Compared with Fig. 15(b), the wave coefficient is improved, and the current ripple is reduced.

The output current of Y-connected winding with the SHEPWM-SC control scheme is shown in Fig. 10(d). The 12n±1(n=1, 2, 3)-order current harmonic amplitudes with SPWM, SHEPWM-DC, and SHEPWM-SC are shown in Table II. With SPWM, the converted input current 11th, 13th, 23rd harmonics are greater than those with SHEPWM-DC and SHEPWM-SC. Its 11th harmonic amplitude is 126.55 A, which is 10.1 times that of SHEPWM-DC and 18.6 times that of SHEPWM-SC. The size of each harmonic component with SHEPWM-SC is the smallest among all the sizes of harmonic components. Similar results are obtained in the simulation.

VII. CONCLUSION

In a medium-voltage high-power converter, grid-side harmonics are affected by several key factors. Through an analysis of these factors, a grid-friendly control strategy was developed.

1) A combined harmonic elimination method that includes a dual primary-side series-connected winding transformer and the SHEPWM scheme was introduced to eliminate $12k \pm 1 (k = \frac{T-1}{2})$-order harmonics and those below the transformer primary-side and secondary-side currents.
2) A synthetic compensation control strategy for three-level medium-voltage high-power converters was proposed to eliminate the grid-side current distortion resulting from dead time and DC magnetic bias in low-switching-frequency application.

The simulation and experimental results validate the control strategy. Compared with the SPWM method, the proposed SHEPWM-SC method reduces the 11th, 13th, and 23rd current harmonics to 5.38%, 2.85%, and 20.31%, respectively. The secondary-side line current THD is improved from 8.62% to 2.21% at a rated operating condition.

ACKNOWLEDGMENT

This paper was supported in part by the National Science Foundation of China under grants 61473314 and 61403425 and by the National Science Foundation of China through the Science Foundation of Innovation Research Group under grant 61321003.

REFERENCES

[1] K.-M. Kwon, J.-M. Lee, J.-M. Lee, and J.-H. Choi, "SVPWM Overmodulation scheme of three-level inverters for vector controlled induction motor drives," *Journal of Power Electronics*, Vol. 9, No. 3, pp. 481-490, May 2009.

[2] L. Dalessandro, S. D. Round, U. Drofenik, and J. W. Kolar, "Discontinuous space-vector modulation for three-level PWM rectifiers," *IEEE Trans. Power Electron.*, Vol. 23, No. 2, pp. 530-542, Mar. 2008.

[3] J. D. B. Ramirez, J. J. R. Rivas, and E. Peralta-Sanchez, "DSP-based simplified space-vector PWM for a three-level VSI with experimental validation," *Journal of Power Electronics*, Vol. 12, No. 2, pp. 285-293, Mar. 2012

[4] F. Wang, "Sine-triangle versus space-vector modulation for three-level PWM voltage-source inverters," *IEEE Trans. Ind. Appl.*, Vol. 38, No. 2, pp. 500-506, Mar./Apr. 2002.

[5] Z. Ye, Y. Xu, F. Li, X. Deng, and Y. Zhang, "Simplified PWM strategy for neutral-point-clamped (NPC) three-level converter," *Journal of Power Electronics*, Vol. 14, No. 3, pp. 519-530, May 2014.

[6] J. K. Steinke, "Switching frequency optimal PWM control of a three-level inverter," *IEEE Trans. Power Electron.*, Vol. 7, No. 3, pp. 487-496, Jul. 1992.

[7] R. M. Tallam, R. Naik, and T. A. Nondahl. "A carrier-based PWM scheme for neutral-point voltage balancing in three-level inverters," *IEEE Trans. Ind. Appl.*, Vol. 41, No. 6, pp. 1734-1743, Nov./Dec. 2005.

[8] N. Li, Y. Wang, W. Lei, R. Niu, and Z. Wang, "Novel carrier-based PWM strategy of a three-level NPC voltage source converter without low-frequency voltage oscillation in the neutral point," *Journal of Power Electronics*, Vol. 14, No. 3, pp. 531-540, May 2014.

[9] K. Imarazene, E. M. Berkouk, and H. Chekireb, "Selective harmonics elimination PWM with sel-balancing capacitors in three-level inverter," in *6th IET International Conference on Power Electronics, Machines and Drives (PEMD)*, pp. 1-6, Mar. 2012.

[10] J. Napoles, R. Portillo, J. I. Leon, M. A. Aguirre, and L. G. Franquelo, "Implementation of a closed loop SHMPWM technique for three level converters," in *34th Annual Conference of IEEE Industrial Electronics (IECON)*, pp. 3260-3265, Nov. 2008.

[11] J. A. Pontt, J. R. Rodríguez, A. Liendo, and P. Newman, "Network-friendly low-switching-frequency multipulse high-power three-level PWM rectifier," *IEEE Trans. Ind. Electron.*, Vol. 56, No. 4, pp. 1254-1262, Apr. 2009.

[12] J. Rodríguez, J. Pontt, R. Huerta, and P. Newman, "24-pulse active front end rectifier with low switching frequency," in *IEEE 35th Annual Power Electronics Specialists Conference(PESC)*, Vol. 5, pp. 3517-3523, Jun. 2004.

[13] T. Nakajima, H. Suzuki, K. Izumi, and S. Sugimoto, "A converter transformer with series-connected line-side windings for a DC link using voltage source converters," in *IEEE Power Engineering Society 1999 Winter Meeting*, Vol. 2, pp. 1073-1078, Feb. 1999.

[14] Z. Xi and S. Bhattacharya, "STATCOM operation under single line-ground system faults with magnetic saturation in series connected transformers based 48-pulse voltage-source converter," in *European Conference on Power Electronics and Applications*, pp. 1-10, Sep. 2007.

[15] H. Li, F. C. Lin, and Z. Gui, "Model test for harmonic characteristics of convertor transformer under Dc bias," in *International Conference on Electrical Machines and Systems(ICEMS)*, pp. 4436-4439, Oct. 2008.

[16] L. Zeng, Z. Zhu, B. Bai, and Y. Song, "Research on influence of DC magnetic bias on a converter transformer," in *International Conference on Electrical Machines and Systems(ICEMS)*, pp. 1346-1349, Oct. 2007.
[17] Y. Li, L. Luo, D. He, and C. Rehtanz, "Study on the effects of the DC bias on the harmonic characteristics of the new converter transformer," in *Asia-Pacific Power and Energy Engineering Conference(APPEEC)*, pp. 1-4, Mar. 2010.
[18] G. Mei, Y. Liu, and M. Guo, "Study of transformer's harmonic characteristic in DC magnetic bias," in *China International Conference on Electricity Distribution (CICED),* pp. 1-4, Dec. 2008.
[19] I. Dolguntseva, R. Krishna, D. E. Soman, and M. Leijion, "Contour based dead-time harmonic analysis in a three-level neutral point clamped inverter," *IEEE Trans. Ind. Electron.*, Vol. 62, No. 1, pp. 203-210, Jan. 2015.
[20] H. Mese and A. Ersak, "Compensation of dead-time effects in three-level neutral point clamped inverters based on space vector PWM," in *International Aegean Conference on Electrical Machines and Power Electronics and 2011 Electromotion Joint Conference(ACEMP),* pp. 101–108, Sep. 2011.
[21] J. Gao, T. Q. Zheng, and F. Lin, "Improved deadbeat current controller with a repetitive-control-based observer for PWM rectifiers," *Journal of Power Electronics,* Vol. 11, No. 1, pp. 64-73, Jan. 2011.
[22] J. Xiaomei, R. Yannian, C. Guoqiang, and L. Kaiqiang, "Restraining DC magnetic bias in PS-PWM full bridge inverter of plasma power," in *International Conference on Intelligent System Design and Engineering Application (ISDEA),* Vol. 2, pp. 306-309, Oct. 2010.
[23] J. Gao, X. Zhao, X. Yang, and Z. Wang, "The research on avoiding flux imbalance in sinusoidal wave inverter," in *the Third International Power Electronics and Motion Control Conference,* Vol. 3, pp. 1122–1126, Aug. 2000.
[24] T. Nakajima, K.-I. Suzuki, M. Yajima, and N. Kawakami, "A new control method preventing transformer DCmagnetiz ation for voltage source self-commutatedconverters," *IEEE Trans. Power Del.*, Vol. 11, No. 3, pp. 1522-1528, Jul. 1996.
[25] W. C. Bloomquist, "Select the right transformer winding connection for industrial power systems," *IEEE Trans. Ind. Appl.,* Vol. IA-11, No. 6, pp. 641-645, Nov. 1975.
[26] X. Liang, W. Jackson, and R. Laughy, "Transformer winding connections for practical industrial applications," in *IEEE Petroleum and Chemical Industry Technical Conference(PCIC)*, pp. 1-9, Sep. 2007.
[27] B.-R. Lin, "Implementation of a ZVS three-level converter with series-connected transformers," *Journal of Power Electronics,* Vol. 13, No. 2, pp. 177-185, Mar. 2013.

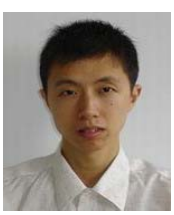

Jing Shang was born in Sichuan Province, China, in 1977. He received his B.Sc. degree in mechanical engineering in 2000 and his M.Sc. degree in electric system and automation in 2003 from Southwest Jiaotong University, China. He is currently working toward his Ph.D. degree at the School of Information Science and Engineering, Central South University, Changsha, China. His current research interests include control methods for high-power converters and optimal pulse-width modulation techniques.

Xiaohong Nian was born in Gansu, China, in 1965. He received his B.Sc., M.Sc., and Ph.D. degrees from Northwest Normal University, Shandong University, and Peking University in 1985, 1992, and 2004, respectively. He was a research fellow at the Institute of Zhuzhou Electric Locomotive from 2004 to 2008. He is currently a professor and an editor at Converter Technology & Electric Traction. His research interests are coordinated control and optimization of complicated multi-agent systems, converter technology, and drive control.

Tao Chen was born in Hunan, China, in 1983. He received his B.Sc. and M.Sc. degrees in electrical engineering from Southwest Jiaotong University, Chengdu, China, in 2006 and 2009, respectively. He is currently with CRRC Zhuzhou Institute Co., Ltd., Hunan, China. His main research interests include control strategies in grid side and electric power quality.

Zhenyu Ma was born in Hunan, China, in 1977. He received his M.Eng. degree in computer engineering from Central South University, Changsha, China, in 2007 and his Ph.D. degree in electrical engineering and electronics from Loughborough University, Leicestershire, U.K., in 2012. He worked for Power Systems Warehouse, U.K., from October 2011 to January 2013. He is currently with CRRC Zhuzhou Institute Co., Ltd., Hunan, China. His main research interests include power electronics, high-power converters, and renewable energy, particularly wind power systems.